ORNL/TM-2016/449

Bison Modeling of SiC/SiC Cladding Including Fuel-Pellet Interaction

Fuel Cycle Research & Development Advanced Fuels Campaign

Gyanender Singh
Ryan Sweet
Brian Wirth
Kurt Terrani
Yutai Katoh

Prepared for
U. S. Department of Energy
Office of Nuclear Energy

August 26, 2016
M3FT-16OR020205031

ORNL/TM-2016/449

US DOE Fuel Cycle Research and Development Advanced Fuels Campaign

BISON MODELING OF SIC/SIC CLADDING INCLUDING FUEL-PELLET INTERACTION

Gyanender Singh
Ryan Sweet
Brian Wirth
Kurt Terrani
Yutai Katoh

Date Published: August 26, 2016

Prepared by
OAK RIDGE NATIONAL LABORATORY
Oak Ridge, TN 37831-6283
managed by
UT-BATTELLE, LLC
for the
US DEPARTMENT OF ENERGY
under contract DE-AC05-00OR22725

CONTENTS

LIST OF FIGURES

LIST OF TABLES

ACKNOWLEDGMENT

The authors would like to thank the BISON and MOOSE code developers for their technical support for this work. The high-performance computing facilities made available by Idaho National Laboratory are gratefully acknowledged. Research is sponsored by the Advanced Fuels Campaign of the Fuel Cycle R&D program, Office of Nuclear Energy, US Department of Energy, under contract DE-AC05-00OR22725 with UT-Battelle, LLC.

ABSTRACT

SiC/SiC composites are considered leading candidates for accident tolerant fuel cladding in light water reactors. However, when SiC-based materials are exposed to neutron irradiation, they experience significant changes in dimensions and physical properties. In the extreme nuclear reactor environment, SiC-based fuel cladding will see neutron damage, significant heat flux, as well as a corrosive environment. In this report, we evaluate the effect of non-uniform changes in the dimensions caused by neutron irradiation with variable temperatures, along with the closing of the fuel – clad gap, on the stress development in the clad over the course of time. To ensure reliable and safe operation of accident tolerant fuel cladding concepts such as SiC-based materials, it is important to assess its thermo-mechanical performance under in-reactor conditions of irradiation and realistic temperature distributions. In this work, we have used the BISON fuel performance modeling code to perform the thermo-mechanical analysis of SiC/SiC cladding. A constitutive model is constructed and solved numerically to predict the stress distribution and variation in the cladding under normal operating conditions. The dependence of dimensions and physical properties variation with irradiation and temperature has been incorporated. These initial results from the analyses provides insights about the stress distribution and variation with time in the cladding as well as the interaction of fuel pellet with the cladding under different conditions of initial fuel pellet-cladding gap and steady state power levels.

1. INTRODUCTION

The Fukushima Daiichi nuclear power plant accident in 2011 highlighted the susceptibility of the light water reactor (LWR) cores to severe degradation under beyond-design-basis accident conditions. Efforts to enhance the safety of nuclear power plants are underway and involve extensive research and development work on enhancing the accident tolerance of fuel-cladding system. A number of advanced fuel-cladding systems are under consideration with the primary focus on enhanced steam oxidation resistance [1]. One leading concept involves replacement of Zr-based alloys as fuel cladding with SiC-based materials given their exceptional resistance to steam oxidation; roughly two orders of magnitude lower up to at least 1700°C [2, 3]. Within the SiC category there are several concepts, all of which contain continuous SiC fiber SiC matrix (SiC/SiC) composites and may also contain a monolithic SiC or a metal layer on the inside and/or outside as layered structures. The work presented here focusses on a fully SiC/SiC composite cladding concept, though it may be easily adjusted to take into account the mechanical effects of a monolithic SiC layer or metal coatings in addition to the SiC/SiC composite layer in a layered structure.

The SiC/SiC composite material offers the advantages of both composite and ceramic materials: it maintains high strength and chemical inertness in high-temperature steam like that of the ceramic material [2] and provides good damage tolerance with the high fracture toughness of a composite material. A number of related studies have examined various aspects that need to be considered for deployment of SiC-based materials in LWRs, including neutronics [4, 5] and high-temperature water corrosion [6-8]. In the early stages of development of this material ceramic grade Nicalon^{TM} fibers were not stable under neutron irradiation. Later on fibers with high crystallinity and purity could be manufactured (Nicalon Type S and Tyranno SA) and these fibers were found to be more stable under irradiation [9, 10], thus opening the potential of SiC/SiC composite for nuclear applications. As a result of their properties, the nuclear grade SiC/SiC composites (composites with enhanced resistance to irradiation damage) are being considered an attractive choice for several nuclear applications [11]. A comprehensive discussion on the properties of SiC/SiC composite is provided elsewhere [12].

Thermo-mechanical analysis of SiC-based cladding has received ample attention in the past. The early studies provided useful information regarding the effect of swelling on expansion of fuel-pellet gap and delay of hard contact between the two [13, 14]. These studies also highlighted the large temperature drop across the cladding thickness and the corresponding rise in fuel pellet temperature that leads to additional fission gas release. The latter studies captured the strong temperature dependence on swelling that was neglected earlier [15-17]. The strain associated with this differential swelling was shown to dominate the stress profile in the cladding soon after the onset of irradiation. This profile differs widely from metallic cladding.

The current work focuses on the thermo-mechanical analysis of SiC/SiC cladding with spatially variable boundary conditions (i.e. large axial variation in power, neutron flux, and coolant temperature) as typically present in pressurized water reactors (PWRs). Besides evaluating the stress distribution and variation in the cladding, the study also investigates the interaction of fuel pellet with the cladding under different conditions of fuel pellet-cladding gap and steady state power levels. BISON, a finite-element-based nuclear fuel performance code, is used for performing this study.

2. METHOD

2.1 CONSTITUTIVE MODEL

Several factors contribute to the deformation of SiC/SiC composites under irradiation and high temperature. The strain corresponding to irradiation-induced dimensional change is denoted here as the swelling strain ($\boldsymbol{\varepsilon}^s$). Note that swelling is defined as expansion of material under irradiation in the absence of stress and is considered isotropic for SiC. Swelling of SiC, which saturates early at around ~1 dpa, exhibits strong temperature dependence within a range of LWR fuel cladding-relevant temperatures. Non-uniform swelling in the cladding due to non-uniform temperature thus causes build-up of stresses in the structure. These stresses cause the material to experience irradiation creep. Thermal creep is essentially nonexistent in SiC at temperatures relevant to LWR fuel cladding application [18].

The irradiation creep strain is denoted as $\boldsymbol{\varepsilon}^c$. Due to variation in the temperature and irradiation-induced change in the thermal properties, the material undergoes expansion/contraction resulting in thermal strain ($\boldsymbol{\varepsilon}^{th}$). Besides the swelling, creep and thermal expansion/contraction the material also undergoes elastic deformation which is accounted for by the elastic strain ($\boldsymbol{\varepsilon}^e$). Thus, the total strain is composed of the elastic strain, swelling strain, creep strain and thermal strain. For solving the model numerically, the elastic strain is obtained from total strain ($\boldsymbol{\varepsilon}^{total}$) which is expressed as sum of all these strains. The stresses ($\boldsymbol{\sigma}$) and their increments ($\Delta\boldsymbol{\sigma}$) are obtained using the elastic strain according to the Hooke's law of linear elasticity. The equations 1, 2 and 3 show the mathematical relations between the strains and stresses.

$$\boldsymbol{\varepsilon}^{total} = \boldsymbol{\varepsilon}^e + \boldsymbol{\varepsilon}^c + \boldsymbol{\varepsilon}^s + \boldsymbol{\varepsilon}^{th} \quad (1)$$

$$\boldsymbol{\sigma} = \mathbf{D}\boldsymbol{\varepsilon}^e \quad (2)$$

$$\Delta\boldsymbol{\sigma} = \check{\mathbf{D}}\Delta\boldsymbol{\varepsilon}^e + \Delta\mathbf{D}\boldsymbol{\varepsilon}^e \quad (3)$$

D is the elastic stiffness matrix. Since the Young's modulus is dependent upon irradiation dose and temperature, **D** is a function of dose and temperature. $\check{\mathbf{D}}$ is the mean elastic stiffness matrix during the numerical solution step increment. The dependence of the strains and physical properties on the temperature and irradiation dose for the SiC/SiC composite material have been obtained from the existing literature. The next section discusses these properties.

2.2 MATERIAL PROPERTIES

Table 1 shows the dependence of material properties on irradiation dose and temperature, considered in this analysis.

Table 1: Dependence of material properties of cladding on irradiation and temperature.

Material property	Irradiation	Temperature
Thermal expansion	X	✓
Creep strain	✓	✓
Swelling strain	✓	✓
Specific heat capacity	X	✓
Thermal conductivity	✓	✓
Young's modulus	✓	✓

Swelling: When SiC/SiC composite is neutron irradiated its physical properties and dimensions change. Within the temperature range of interest for fuel cladding application, the material swells with irradiation dose initially and reaches a saturation point after which no appreciable swelling takes place on further irradiation. An important aspect of swelling of SiC/SiC composite under irradiation is that the saturated swelling level decreases significantly with increase in the irradiation temperature. The cause of swelling has been attributed to point defects and small point defect clusters [19]. The swelling of SiC/SiC composite is very similar to that of CVD SiC [20, 21]. The swelling of CVD SiC is related to the fluence level as:

$$\dot{S} = k_s \gamma^{-1/3} \exp\left(\frac{\gamma}{\gamma_{sc}}\right) \qquad (4)$$

where S is swelling (%), k_s is a temperature-dependent constant, γ is fluence in dpa units and γ_{sc} is the characteristic fluence [22]. Figure 1 shows variation of swelling

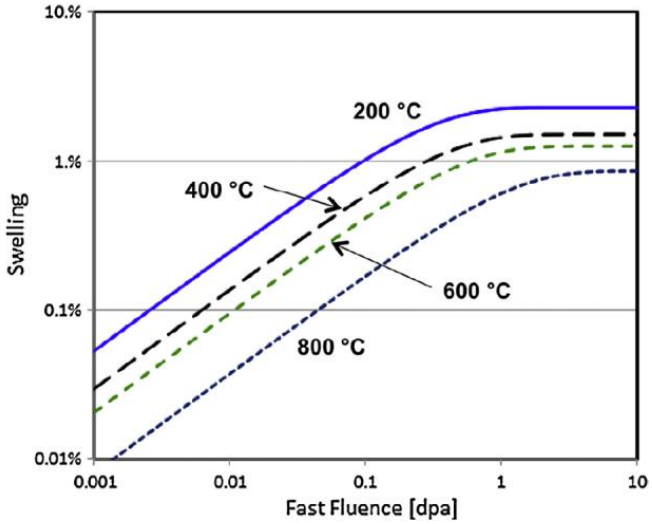

Figure 1: Swelling as a function of dose at different temperature for CVD SiC and CVI SiC/SiC [12].

Creep: SiC/SiC material does not exhibit thermal creep until ~1400°C [18]. Temperature experienced by the cladding in light water reactors is much lower. Katoh et al. showed linear coupling between the irradiation creep and swelling to be a reasonable representation of the experimental data. Accordingly, the irradiation creep strain rate ($\dot{\boldsymbol{\varepsilon}}^{c}$), normalized with stresses is proportional to the swelling rate ($\dot{\boldsymbol{\varepsilon}}_{v}^{s}$) and stress ($\boldsymbol{\sigma}$) [22]:

$$\dot{\boldsymbol{\varepsilon}}^{c} = K\boldsymbol{\sigma}\dot{\boldsymbol{\varepsilon}}_{v}^{s} \qquad (5)$$

where K is a temperature dependent constant.

Thermal conductivity: Tyranno SA3 (SA3) fiber and Hi-Nicalon Type-S (HNLS) fiber based composites show wide variation in their room temperature thermal conductivity in the through-thickness direction: 8.5 – 18.1 W/m K for HNLS and 15.2 – 23.7 W/m K for SA3 composites [12]. For the current work through-thickness thermal conductivity of 2D fabric layup of SA3 composite is employed. CVI SiC is the matrix material with the pyrocarbon as interphase. Since the through-thickness conductivity is largely affected by porosity of the material the value of thermal conductivity used here may be an underestimate.

When SiC/SiC composite is exposed to neutron irradiation the thermal conductivity decreases steeply and reaches saturation within few dpa of fast neutron fluence. This drop in the thermal conductivity under irradiation [23-28] has been attributed to the generation of defects and defect clusters which effectively scatter phonons. The net thermal resistivity (reciprocal thermal conductivity) can be expressed as a sum of thermal resistivity of the unirradiated material and increment in the thermal resistivity due to created defects [29].

$$K_{irr}^{-1} = K_{o}^{-1} + K_{rd}^{-1} \qquad (6)$$

K_{irr}^{-1}: Thermal resistivity of irradiated material
K_{o}^{-1}: Thermal resistivity of unirradiated material
K_{rd}^{-1}: Radiation defect thermal resistivity

The thermal resistivity of unirradiated materials is (based on [12]):

$$K_{o}^{-1} = \frac{190.32T + 36684.0}{\rho_{o}C_{p}} \qquad (7)$$

where
ρ_{o}: Initial density (kg/m^3)
C_{p}: Specific heat capacity (J/kgK)

The defect thermal resistivity of CVD SiC has been found to be proportional to irradiation induced swelling [30]. Based on defect thermal resistivity – irradiation temperature data [12] [20, 31] and swelling – temperature data [19], defect thermal resistivity relates to swelling strain as:

$$K_{rd}^{-1} = 14.275\ \varepsilon_{v}^{s} \qquad (8)$$

Young's modulus and Poisson's ratio: As mentioned earlier, for a linear elastic material the stress is related to the strain through the Hooke's law as:

$$\boldsymbol{\sigma} = D\boldsymbol{\varepsilon}^{e}$$

where **D** is the elastic stiffness of the material. Young's modulus of CVD SiC has been found to slightly decrease with increase in the irradiation induced swelling [19]. Since the swelling of SiC/SiC composite is very similar to that of CVD SiC [20, 21], the effect of neutron irradiation on the Young's modulus for SiC/SiC composite is assumed to be same as that for CVD SiC material. The weakening effect of irradiation on the elastic stiffness of SiC/SiC composite can be written as:

$$\mathbf{D} = \mathbf{D}_o(1 - 6\varepsilon_v^s) \qquad (9)$$

where $\mathbf{D_o}$ and **D** are the elastic stiffness of the unirradiated and irradiated material respectively. The elastic stiffness decreases by about 10% over the period of 2 years.

Specific heat capacity: Specific heat capacity of SiC/SiC composite is considered identical to that of monolithic CVD SiC which does not vary significantly with irradiation dose. The dependence of specific heat capacity on temperature is well established [32-34] in the literature and has been incorporated in the current analysis.

Coefficient of thermal expansion (CTE): The effect of irradiation dose on the CTE has been found to be insignificant. However, CTE has been found to increase monotonically with temperature [12]. The CTE employed is this work is based on the data presented in reference [12].

2.3 ANALYSIS

The fuel performance finite element code BISON [35] was used to perform the thermo-mechanical analysis. An axisymmetric model of the fuel pellet and cladding was analyzed. A section of the fuel pellet and cladding is shown in Figure 2. The geometric dimensions for the model were representative of the Westinghouse AP1000 PWR and are shown in Table 2. Second order quadrilateral elements with 8 nodes were used to generate the mesh of the pellet and cladding. Cladding was meshed with 5 elements in the radial direction and 900 elements in the axial direction. Fuel pellet was meshed with 11 elements in the radial direction and 1500 elements in the axial direction.

Table 2: Dimensions of the fuel-pellet and cladding considered in the analysis.

Geometry	Dimension
Cladding outer radius	4.75 mm
Cladding thickness	572 μm
Cladding height	4.0 m
Fuel pellet stack height	3.658 m
Top plenum gap height	0.232 m
Bottom plenum gap height	0.105 m

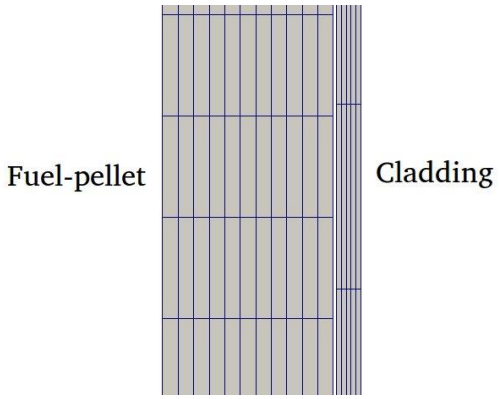

Figure 2: A section of the axisymmetric finite element model of fuel pellet and cladding.

The initial plenum pressure was set to 2 MPa. An external pressure at 15 MPa, generated due to pressurized coolant was applied at the external surface of the cladding. A thermal boundary condition for heat loss due to convection was applied at the external surface. These boundary conditions can be expressed as:

$$k\nabla \mathbf{T} = \mathbf{q} = h(T - T_c) \qquad (10)$$

where k, T and q represent thermal conductivity, temperature and heat flux respectively; convective heat transfer coefficient h = 30 kW/m^{2}K and coolant temperature T_c. Figure 3 shows the axial power profile considered in the analysis. The contact was modeled to be 'Frictionless' in these analyses. However, for understanding the effect of type of contact model ('Frictionless' and 'Glued') on the stresses some analyses were performed with 'Glued' model of contact.

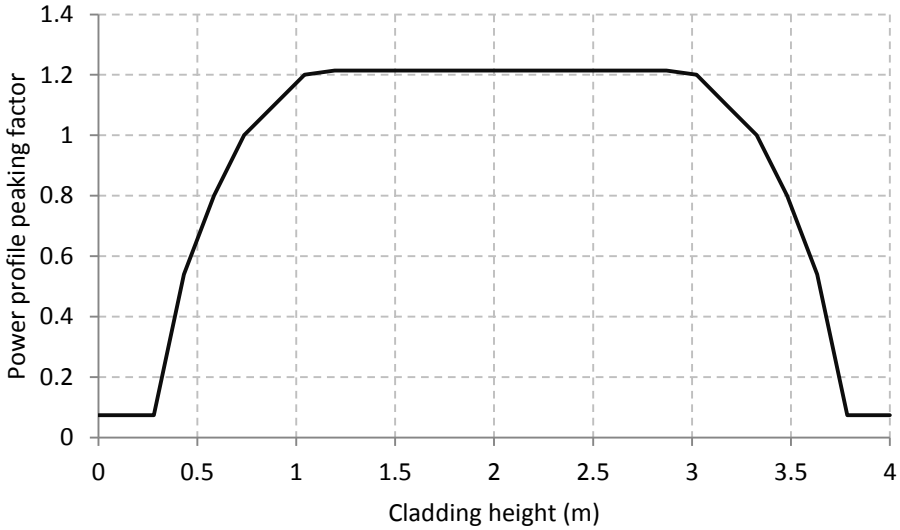

Figure 3: Axial power profile considered in the analysis.

3. RESULTS AND DISCUSSION

3.1 GAP CLOSURE – DEPENDENCE ON POWER AND INITIAL GAP THICKNESS

The analyses were performed for different steady state power (18kW/m, 22kW/m, 26kW/m and 30kW/m) and initial gap thicknesses (50µm, 65µm, 80µm and 95µm). Figure 4 shows the variation of fuel pellet-cladding gap thickness with burnup for different steady state power levels and initial gap thicknesses. Table 2 lists the burnup level at gap closure for each power level and initial gap thicknesses considered in the analysis. Two initial conclusions can be drawn from the data: 1) a larger initial pellet-cladding gap closes after a larger burnup and 2) gap closure is significantly delayed for lower steady-state power level. For power level of 18 kW/m, the burnup at gap closure increases by about 9 MWd/kg/UO_2 for every 15µm increase in the initial gap thickness. The corresponding increase in the burnup at gap closure for power levels of 22 kW/m, 26 kW/m and 30 kW/m is 6 MWd/kg-UO_2, 2.5 MWd/kg-UO_2 and 0.7 MWd/kg-UO_2, respectively. As shown in Table 2, for a fixed initial gap thickness, the rise in steady state power level increases the rate of the gap closure.

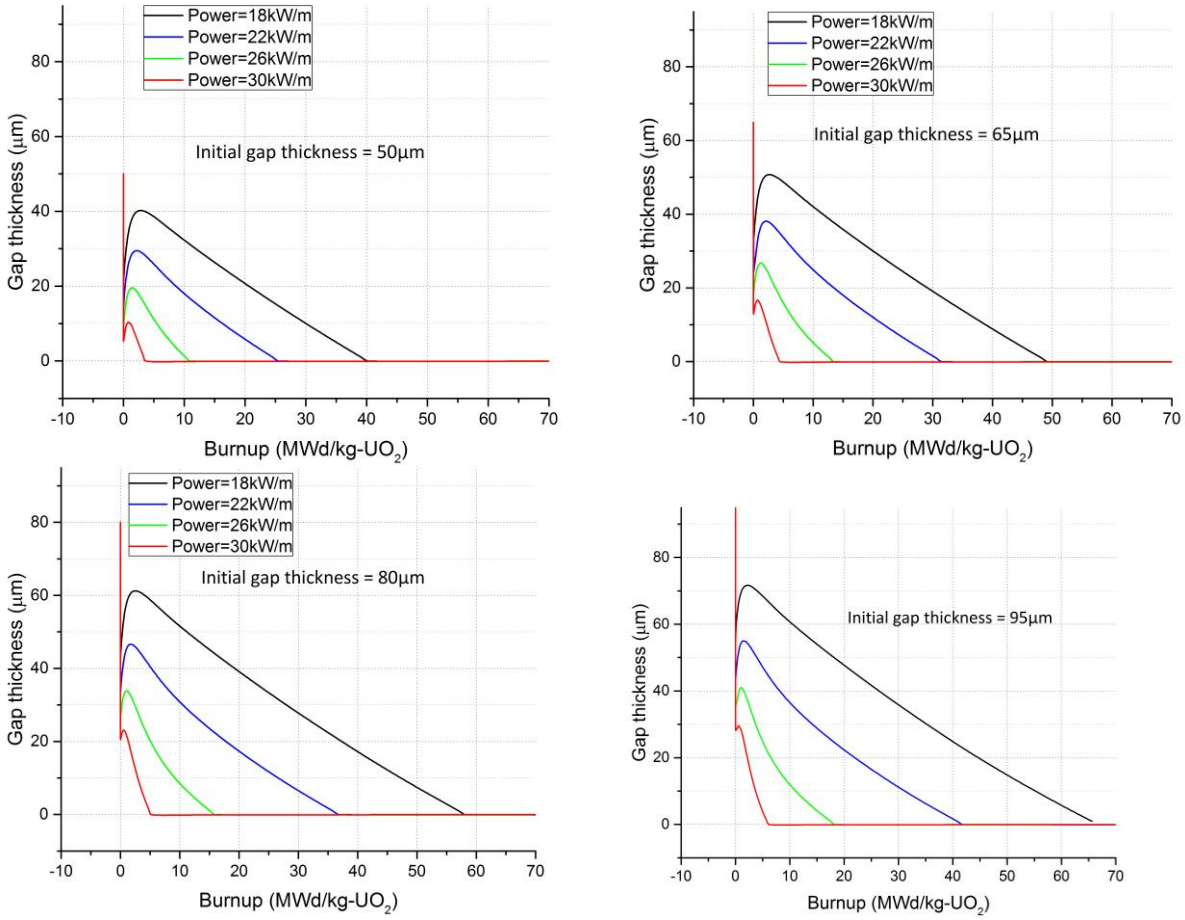

Figure 4: Gap thickness as a function of burnup for different steady-state power levels and initial gap thickness.

Table 3: Burnup (MWd/kg-UO_2) at gap closure for different steady-state power levels and initial gap thicknesses.

Initial gap thickness (μm)	Power = 18 kW/m	Power = 22 kW/m	Power = 26 kW/m	Power = 30 kW/m
50	40.0	25.4	10.8	3.7
65	49.1	31.2	13.4	4.5
80	58.0	36.7	15.9	5.1
95	67.0	41.7	18.1	5.9

It can be noted from Figure 4 that there is a significant decrease in the fuel-pellet gap at the startup of the reactor. For instance, the initial gap of 50 μm decreases to about 5 μm for power level of 30 kW/m. This decrease in the gap is caused by the fuel thermal expansion. Although the cladding also experiences thermal expansion, the combination of much lower temperatures in the cladding and smaller CTE for SiC compared to UO_2 results in much smaller radial expansion compared to the pellet. For higher power levels the decrease in the gap thickness is greater due to higher fuel temperature. After the initial decrease in the pellet-cladding gap thickness, the gap thickness increases. This increase in the gap thickness is caused by the swelling of SiC/SiC cladding under neutron irradiation as discussed previously in section 2.2. When the swelling in the cladding becomes saturated (~ 1 dpa) the pellet-cladding gap decreases constantly due to fuel pellet swelling (steady-state swelling due to fission products). The next section discusses the effect of fuel thermal expansion in greater detail.

3.2 EFFECT OF FUEL THERMAL EXPANSION ON GAP CLOSURE

Analyses were performed with the exclusion of fuel thermal expansion to understand how significantly fuel thermal expansion influences gap closure. Figure 5 shows the variation of gap thickness as a function of burnup with and without the inclusion of fuel thermal expansion, for a case with initial gap thickness of 80μm. As seen in Figure 5, fuel thermal expansion has a significant effect on the gap closure time for cases with lower power levels. Gap closure occurs after about 1.5 – 2 times larger burnup when fuel thermal expansion is not incorporated in the analysis, as compared to the case when fuel thermal expansion is included.

When the fuel thermal expansion is not included, the greater gap thickness leads to higher temperatures in the fuel pellet. For instance, the fuel pellet is at about 350 K higher temperature for the case with initial gap thickness of 50 μm and power level of 30 kW/m. The higher temperature leads to greater gaseous swelling of the fuel pellets, thus, compensating for the assumed lack of fuel thermal expansion. The greater gaseous swelling is particularly applicable for cases with higher power levels. Thus, excluding the fuel thermal expansion does not lead to significant delay in gap closure for cases with higher power levels. In any case, any enhancement in UO_2 thermal conductivity would have the benefit of reduced pellet temperature that in turn results in less thermal expansion and swelling, thereby delaying the gap closure. The next section discusses the stress state in the cladding.

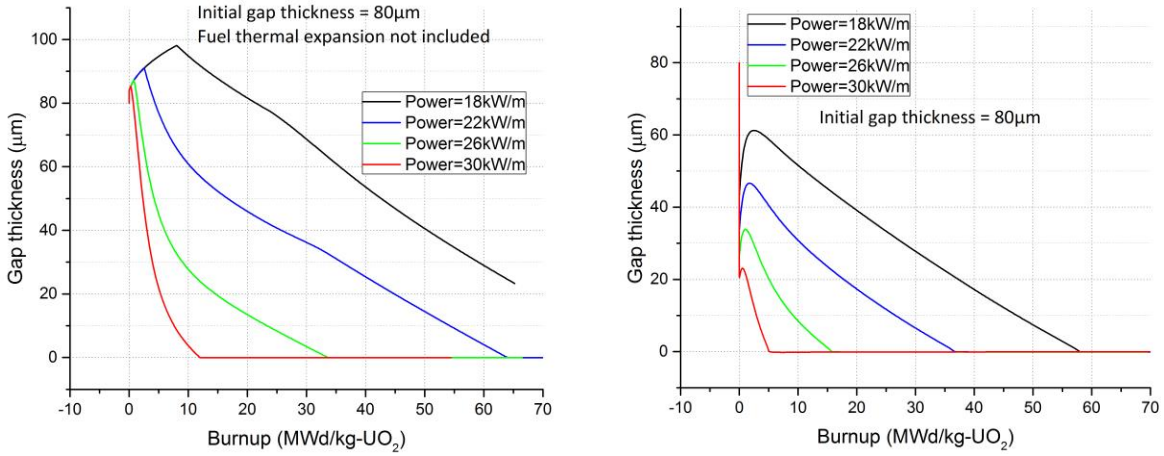

Figure 5: Gap thickness as a function of burnup for the cases when the fuel thermal expansion is not included (left) and when it is included (right).

3.3 STRESS STATE IN THE CLADDING

This section discusses the stress distribution and variation in the cladding (initial pellet-cladding gap thickness = 80 μm). Figures 6 – 8 show the variation of hoop, axial and radial stresses in the cladding, respectively, as a function of time. Figures 9 and 10 show the variation of hoop and axial stresses along the height of the cladding at the end of two years. Figure 11 shows the variation of temperature with height at the outer and inner surface of the cladding after 2 years. As discussed earlier the contact between the fuel-pellet and cladding is delayed considerably for lower steady state power levels. These results are presented for two power levels, 18 kW/m and 26 kW/m, with the motivation to understand the effect of contact between the fuel-pellet and cladding on the stresses.

At the reactor startup, both hoop and axial stresses are compressive because of the external pressure of 15 MPa in the PWR coolant. At this time the inner region of the cladding is at a higher temperature than the outer region and correspondingly, the inner region of the cladding expands more than the outer region. The outer region, which experiences less expansion, prevents the inner region from expanding. Thus, the inner region of the cladding is under higher compressive stresses relative to the outer region of the cladding.

As time progresses the SiC/SiC composite material experiences volumetric expansion due to neutron irradiation, and this swelling is inversely related to the temperature: swelling is smaller at higher temperature. The inner region, being at higher temperature, swells less than the outer region. So, although the net expansion (thermal expansion and swelling) of the inner region of the cladding was greater than that of the outer region at the beginning of operation, after some time ($t \approx 2$ weeks) the net expansion of the outer region becomes greater. This variation leads to higher compressive stress in the outer region of the cladding relative to the inner region. As the difference in the swelling magnitude increases, the difference in the stress levels in the inner and outer layers rises. When swelling saturates, the difference in the stress levels becomes steady and do not increase further with time. However, due to continuous release of fission gas, the internal pressure rises. This continuous increase in the internal pressure causes stress level to rise steadily even after swelling saturates. It may be noted that for higher power level of 26

kW/m fission gas is released at a higher rate, thus, both hoop and axial stresses increase more rapidly than that for the case with lower power level of 18 kW/m.

The variation in the axial stresses with time is similar to that of hoop stress with the exception that the rate of increase of the axial stress is smaller than that of the hoop stress. This can be explained through the relation of stress with the internal pressure for thin-walled cylindrical structure. Equation 11 and 12 show the relation of hoop stress (σ_{hoop}) and axial stress (σ_{axial}) with internal pressure (p) for a thin-walled tube approximation; r_i is the internal radius and t is the thickness. Equation 13 shows that the rate of increase of hoop stress with internal pressure is twice of that for the axial stress.

$$\sigma_{hoop} = \frac{pr_i}{t} \qquad (11)$$

$$\sigma_{axial} = \frac{pr_i}{2t} \qquad (12)$$

$$\frac{d\sigma_{hoop}}{dp} = 2\frac{d\sigma_{axial}}{dp} \qquad (13)$$

Thus, with the increase in the internal pressure due to fission gas release the hoop stresses rise at a rate about twice of that for axial stresses.

The radial stress at the inner surface is 2 MPa initially and rapidly rises in magnitude with increase in the plenum pressure. The radial stress at the outer surface remains constant at about 15 MPa as the external coolant pressure remains constant. The stress level reported here are measured at the centroid of the element at the outer surface and not exactly at the surface; so stress level deviate slightly from 15 MPa. It can be noted here that the radial stress rise at a much faster rate for steady state power level of 26 kW/m compared to that with power level of 18 kW/m. This is because the fission gas release rate is greater for higher power, thus, the radial stress at the inner surface also rise at a faster rate.

Figure 6 shows a sudden rise in the hoop stresses of about 50 MPa for the case with power level of 26 kW/m at about 0.8 years. This rise in the hoop stress is because of the contact between the cladding and the fuel-pellet. The axial stresses do not show a similar rise as in the hoop stress because the 'Frictionless' contact model allows the fuel pellet to slide freely with respect to the cladding in axial direction without generating any axial stresses in the cladding. The hoop stresses for the case with power level of 18 kW/m do not show similar rapid rise because there is no occurrence of pellet-cladding interaction for this case.

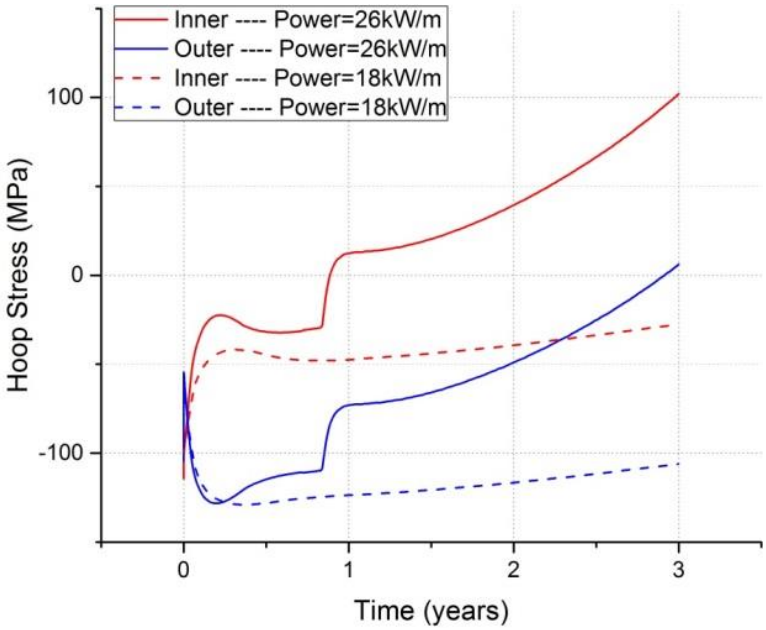

Figure 6: Variation of hoop stress at mid-height plane in the cladding as a function of time.

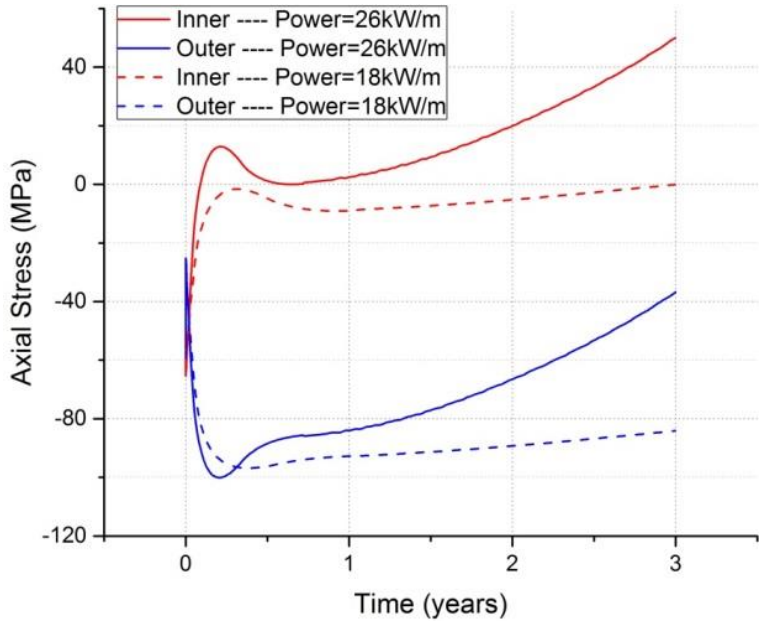

Figure 7: Variation of axial stress at mid-height plane in the cladding as a function of time.

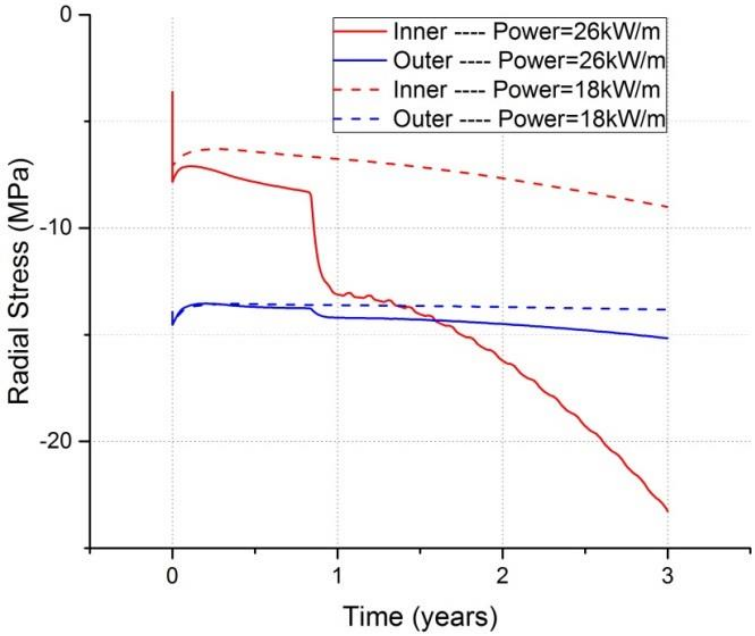

Figure 8: Variation of radial stress at mid-height plane in the cladding as a function of time.

Figure 9 and 10 show the variation of hoop and axial stress along the height of the cladding at the end of 2 years. Figure 11 shows the corresponding variation in the temperature. It can be noted that the stresses for the case with power level of 26 kW/m are much higher. The stresses are higher because for this case the fuel-pellet and cladding are in contact. H1 and H2 labels in Figure 9 indicate the regions of beginning and end of the contact. Consequently the cladding region between H1 and H2 locations show considerable higher stresses than the rest of the cladding.

Figure 9 and 10 also show that the stresses magnitude decreases along the height of the cladding. This can be attributed to the rise in the temperature of the cladding (shown in Figure 11). As described earlier the saturated swelling in the SiC/SiC composite decreases with rise in temperature. Therefore, the swelling gradient along the radial direction, which contributes significantly to the stresses in the cladding, decrease with the height of the cladding. Consequently, the stress magnitude levels also decrease with the cladding height.

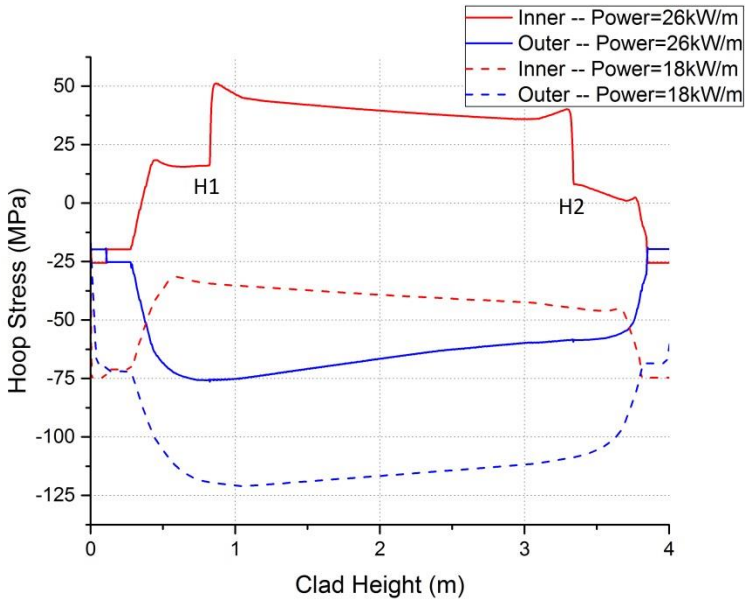

Figure 9: Variation of hoop stress along the height of the cladding for steady state power levels of 18kW/m and 26kW/m at the end of 2 years.

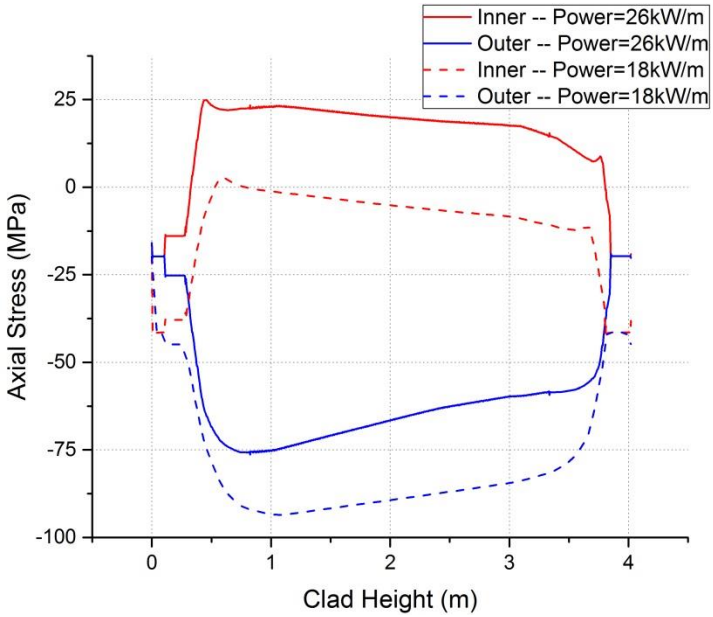

Figure 10: Variation of axial stress along the height of the cladding for steady state power levels of 18kW/m and 26kW/m at the end of 2 years.

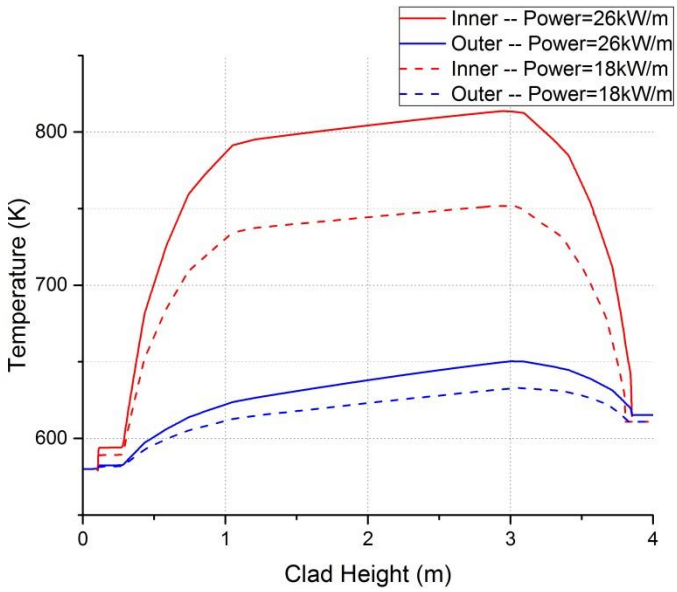

Figure 11: Variation of temperature along the height of the cladding for steady state power levels of 18kW/m and 26kW/m at the end of 2 years.

3.4 CONTACT FORMULATION – FRICTIONLESS VS. GLUED

Analyses were also performed to understand the effect of the contact model on the stress development in the cladding. Two cases, one with the 'Frictionless' contact model and other with 'Glued' contact model, were considered, thus, essentially providing a bounding analysis on the expected clad stress levels. For 'Glued' model the interacting surfaces are not allowed to move relatively after coming in contact while for 'Frictionless' contact the surfaces can slide freely relative to each other without exerting any shear stresses on the other surface. An initial gap thickness of 80 μm and steady state power level of 18 kW/m were considered in the analysis. Figure 12 shows the variation of hoop and axial stress variation with time for the two cases.

As discussed earlier, axial stress does not change due to contact when 'Frictionless' contact model is used. However, the hoop stress rises rapidly by about 50 MPa due to the occurrence of contact. The rate of rise in the hoop stress decreases with time for the 'Frictionless' contact model. After about three months of operation the rise in the hoop stress due to contact becomes insignificant. On the other hand there is rapid rise in both the hoop and axial stresses when 'Glued' contact model is employed. This contact model stops relative movement of fuel pellets with respect to the cladding at the location of contact. The expansion of the fuel pellets makes the claddings inner region also deform along with it, thus, introducing significant stresses in the cladding as shown in Figure 12. Unlike the 'Frictionless' contact model, the rise in the stresses continue with time for the 'Glued' model, leading to very high stress levels in the cladding.

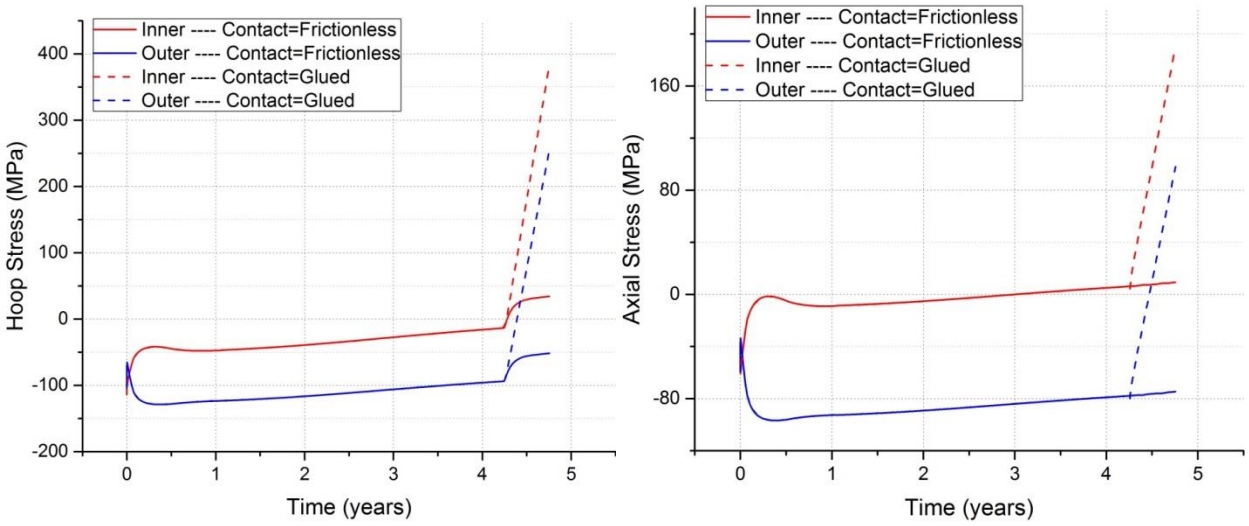

Figure 12: Variation of stresses with time in the cladding for steady state power level of 18kW/m, for two cases of contact type - frictionless and glued.

4. SUMMARY

The work presented herein focused on the thermo-mechanical analysis of SiC/SiC cladding which is considered a leading candidate for accident tolerant fuel cladding systems in light water reactors. These initial results from the analysis showed that the steady state power level and the initial gap thickness between the fuel-pellet and the cladding have a significant impact on the pellet-cladding gap closure time. The lower power levels can significantly delay the pellet-cladding gap closure. It was also found that the fuel thermal expansion significantly decreases the time for pellet-gap closure. The distribution and variation of stresses with time were evaluated. Comparison of cases with and without contact showed that the contact between the pellet and cladding can lead to considerable rise in the stress levels. However, the evaluated stresses are dependent on the type of contact model employed in the numerical simulation. The results from the analyses indicated significant contribution of irradiation induced swelling in the SiC/SiC cladding to the stress development. The dependence of this swelling on temperatures leads to variation in the stress levels along the height of the cladding. These are the initial results and a more rigorous analysis may be needed to ensure that the results indicate the actual performance of the SiC/SiC cladding. This work sets the stage for a 3D pellet-cladding interaction study which will enable understanding the effect of circumferential variation of power profile on the pellet-cladding interaction and stress state in the cladding.

5. REFERENCES

[1] S. J. Zinkle, K. A. Terrani, J. C. Gehin, L. J. Ott, and L. L. Snead, "Accident tolerant fuels for LWRs: A perspective," *Journal of Nuclear Materials,* vol. 448, pp. 374-379, 2014.

[2] K. A. Terrani, B. A. Pint, C. M. Parish, C. M. Silva, L. L. Snead, and Y. katoh, "Silicon Carbide Oxidation in Steam up to 2 MPa," *Journal of American Ceramic Society,* vol. 97, pp. 2331-2352, 2014.

[3] V. A. Avincola, M. Grosse, U. Stegmaier, M. Steinbrueck, and H. J. Seifert, "Oxidation at high temperatures in steam atmosphere and quench of silicon carbide composites for nuclear application," *Nuclear Engineering and Design* vol. 295, pp. 468–478, 2015.

[4] D. A. Bloore, "Reactor physics assessment of thick silicon carbide clad PWR fuels," Massachusetts Institute of Technology, 2013.

[5] N. M. George, K. Terrani, J. Powers, A. Worrall, and I. Maldonado, "Neutronic analysis of candidate accident-tolerant cladding concepts in pressurized water reactors," *Annals of Nuclear Energy,* vol. 75, pp. 703-712, 2015.

[6] K. A. Terrani, Y. Yang, Y.-J. Kim, R. Rebak, H. Meyer, and T. J. Gerczak, "Hydrothermal corrosion of SiC in LWR coolant environments in the absence of irradiation," *Journal of Nuclear Materials,* vol. 465, pp. 488-498, 2015.

[7] S. Kondo, M. Lee, T. Hinoki, Y. Hyodo, and F. Kano, "Effect of Irradiation Damage on Hydrothermal Corrosion of SiC," *Journal of Nuclear Materials,* vol. 464, pp. 36-42, 2015.

[8] D. Kim, H.-G. Lee, J. Y. Park, J.-Y. Park, and W.-J. Kim, "Effect of dissolved hydrogen on the corrosion behavior of chemically vapor deposited SiC in a simulated pressurized water reactor environment," *Corrosion Science* vol. 98, pp. 304–309, 2015.

[9] M. Takeda, J. Sakamoto, A. Saeki, Y. Imai, and H. Ichikawa, "High performance silicon carbide fiber Hi-Nicalon for ceramic matrix composites," in *19th Annual Conference on Composites, Advanced Ceramics, Materials, and Structures-A: Ceramic Engineering and Science Proceedings, Volume 16*, 2009, p. 37.

[10] L. Snead, Y. Katoh, A. Kohyama, J. Bailey, N. Vaughn, and R. Lowden, "Evaluation of neutron irradiated near-stoichiometric silicon carbide fiber composites," *Journal of Nuclear Materials,* vol. 283, pp. 551-555, 2000.

[11] R. Naslain, "Design, preparation and properties of non-oxide CMCs for application in engines and nuclear reactors: an overview," *Composites Science and Technology,* vol. 64, pp. 155-170, 2004.

[12] Y. Katoh, K. Ozawa, C. Shih, T. Nozawa, R. J. Shinavski, A. Hasegawa*, et al.*, "Continuous SiC fiber, CVI SiC matrix composites for nuclear applications: Properties and irradiation effects," *Journal of Nuclear Materials,* vol. 448, pp. 448-476, 2014.

[13] D. M. Carpenter, "An assessment of silicon carbide as a cladding material for light water reactors," Massachusetts Institute of Technology, 2010.

[14] "Falcon-Based Comparative Assessment of Prototype Zr-4 and SiC Fuel Rod, EPRI-1022907," Electric Power Research Institute, Palo Alto, CA2011.

[15] M. Ben-Belgacem, V. Richet, K. A. Terrani, Y. Katoh, and L. L. Snead, "Thermo-mechanical analysis of LWR SiC/SiC composite cladding," *Journal of Nuclear Materials,* vol. 447, pp. 125-142, 2014.

[16] Y. Lee and M. S. Kazimi, "A structural model for multi-layered ceramic cylinders and its

application to silicon carbide cladding of light water reactor fuel," *Journal of Nuclear Materials,* vol. 458, pp. 87-105, 2015.
[17] J. Stone, R. Schleicher, C. Deck, G. Jacobsen, H. Khalifa, and C. Back, "Stress analysis and probabilistic assessment of multi-layer SiC-based accident tolerant nuclear fuel cladding," *Journal of Nuclear Materials,* 2015.
[18] C. CARTER, R. DAVIS, and J. BENTLEY, "Kinetics and Mechanisms of High-Temperature Creep in Silicon Carbide: II, Chemically Vapor Deposited," *Journal of the American Ceramic Society,* vol. 67, pp. 732-740, 1984.
[19] L. L. Snead, T. Nozawa, Y. Katoh, T. S. Byun, S. Kondo, and D. A. Petti, "Handbook of SiC properties for fuel performance modeling," *Journal of Nuclear Materials,* vol. 371, pp. 329-377, 2007.
[20] J. Hegeman, J. Van der Laan, M. Van Kranenburg, M. Jong, D. d'Hulst, and P. Ten Pierick, "Mechanical and thermal properties of SiC f/SiC composites irradiated with neutrons at high temperatures," *Fusion engineering and design,* vol. 75, pp. 789-793, 2005.
[21] Y. Katoh, "Final Report on Irradiation of Bonded-fiber SiC Composite, ORNL/TM-2012/201, Oak Ridge National Laboratory," 2010.
[22] Y. Katoh, L. L. Snead, C. M. Parish, and T. Hinoki, "Observation and possible mechanism of irradiation induced creep in ceramics," *Journal of Nuclear Materials,* vol. 434, pp. 141-151, 2013.
[23] W. Dienst, T. Fett, R. Heidinger, H. Röhrig, and B. Schulz, "Investigations on ceramic materials for fusion technology," *Journal of nuclear materials,* vol. 174, pp. 102-109, 1990.
[24] C. Lee, F. Pineau, and J. Corelli, "Thermal properties of neutron-irradiated SiC; effects of boron doping," *Journal of Nuclear Materials,* vol. 108, pp. 678-684, 1982.
[25] J. Corelli, J. Hoole, J. Lazzaro, and C. Lee, "Mechanical, Thermal, and Microstructural Properties of Neutron-Irradiated SiC," *Journal of the American Ceramic Society,* vol. 66, pp. 529-538, 1983.
[26] R. J. Price, "Thermal conductivity of neutron-irradiated pyrolytic beta-silicon carbide," *Journal of Nuclear Materials,* vol. 46, pp. 268-272, 1973.
[27] D. J. Senor, G. E. Youngblood, J. L. Brimhall, D. J. Trimble, G. A. Newsome, and J. J. Woods, "Dimensional stability and strength of neutron-irradiated SiC-based fibers," *Fusion Technology,* vol. 30, pp. 956-968, 1996.
[28] L. L. Snead, "Limits on irradiation-induced thermal conductivity and electrical resistivity in silicon carbide materials," *Journal of Nuclear Materials,* vol. 329-333, pp. 524-529, 2004.
[29] L. Snead, S. Zinkle, and D. White, "Thermal conductivity degradation of ceramic materials due to low temperature, low dose neutron irradiation," *Journal of nuclear materials,* vol. 340, pp. 187-202, 2005.
[30] L. L. Snead, Y. Katoh, and S. Connery, "Swelling of SiC at intermediate and high irradiation temperatures," *Journal of Nuclear Materials,* vol. 367-370, pp. 677-684, 2007.
[31] Y. Katoh, L. L. Snead, T. Nozawa, T. Kondo, and J. T. Busby, "Thermophysical and mechanical properties of near-stoichiometric fiber CVI SiC/SiC composites after neutron irradiation at elevated temperatures," *Journal of Nuclear Materials,* vol. 403, pp. 48-61, 2010.
[32] K. E. Barrett, M. Teague, I. J. Van Rooyen, S. M. Bragg-Sitton, K. Ellis, C. Glass, *et al.*,

"Engineering challenges of LWR advanced fuel cladding technology in preparation for in-reactor demonstrations," Oak Ridge National Laboratory (ORNL)2012.

[33] A. Collins, M. A. Pickering, and R. L. Taylor, "Grain size dependence of the thermal conductivity of polycrystalline chemical vapor deposited β-SiC at low temperatures," *Journal of applied physics,* vol. 68, pp. 6510-6512, 1990.

[34] M. A. Pickering, R. L. Taylor, J. T. Keeley, and G. A. Graves, "Chemically vapor deposited silicon carbide (SiC) for optical applications," *Nuclear Instruments and Methods in Physics Research Section A: Accelerators, Spectrometers, Detectors and Associated Equipment,* vol. 291, pp. 95-100, 1990.

[35] R. Williamson, J. Hales, S. Novascone, M. Tonks, D. Gaston, C. Permann, *et al.*, "Multidimensional multiphysics simulation of nuclear fuel behavior," *Journal of Nuclear Materials,* vol. 423, pp. 149-163, 2012.